



Microstructure, Mechanical, and Tribological Properties of Amorphous WB₂/Ti Multilayer Coatings

Wenhe Li^{1,2} · Wenshuang Gu^{1,2} · Yuqiu Chen¹ · Jun Gong¹ · Zhiliang Pei¹ · Chao Sun¹

Received: 4 November 2022 / Revised: 12 December 2022 / Accepted: 3 January 2023 / Published online: 16 March 2023
© The Chinese Society for Metals (CSM) and Springer-Verlag GmbH Germany, part of Springer Nature 2023

Abstract

Amorphous WB₂/Ti multilayer coatings with different modulation ratios (1, 5, 15, and 30) and different bilayer numbers (10, 20, 30, 50, and 70) were deposited by direct-current magnetron sputtering. The effect of modulation ratio and bilayer number on the microstructure, mechanical, and tribological properties of WB₂/Ti multilayer coatings was studied systematically. In the investigation for the influence of modulation ratio, the hardness of the multilayer coatings increases with the increment of modulation ratio. The indentation toughness shows a different changing tendency compared to that of the hardness with different modulation ratios. The wear rates of the multilayer coatings with different modulation ratios are at the same level with the influence of both hardness and indentation toughness. In the investigation for the influence of bilayer number, both hardness and indentation toughness increase first and then decrease with an increasing bilayer number. WB₂/Ti multilayer coating with a modulation ratio of 5 and bilayer number of 50 exhibits the highest hardness of 20.4 GPa and lowest wear rate of $1.76 \times 10^{-16} \text{ m}^3/\text{Nm}$. In addition, the hardness strengthening mechanism and wear mechanism of the multilayer coatings were discussed in detail.

Keywords Magnetron sputtering · WB₂/Ti multilayer · Mechanical properties · Tribological properties

1 Introduction

Hard coatings have been required to fulfill the demand of the rapidly growing industries. In recent years, transition-metal diborides (TMB₂), such as TiB₂, CrB₂, and WB₂, have attracted growing attention for hard coatings because of their excellent properties [1, 2, 3, 4, 5]. In the TMB₂ systems, AlB₂-type WB₂ coating has widely followed with interest due to its high hardness (35–45 GPa), high melting point (2560 °C), and good wear resistance, which makes

it an excellent candidate as a protective coating [6, 7, 8, 9, 10, 11, 12]. However, the low toughness of AlB₂-type WB₂ coating and the poor adhesive strength induced by the huge difference in the hardness and thermal expansion coefficient between the coating and substrate, such as cemented carbide, limit its further application in industry. In comparison, amorphous WB₂ coatings exhibit better fracture toughness despite lower hardness.

In order to balance the conflict between the hardness and toughness of hard coatings, some novel concepts have been proposed and widely used, such as nanocomposite and multilayer architecture [13]. Designing multilayer coatings with alternating more than one type of sublayer material has attracted much interest because of its potential to enhance the overall performance of the coatings. Multilayer coatings consisting of ceramic and metallic sublayers combine the high hardness and decent wear resistance of the ceramic sublayers, and the good toughness of the metallic sublayer, allowing the synthesis of coatings with balanced hardness and toughness, such as Ti/TiN [14, 15], Cr/CrN [16, 17], and Ti/TiAlN [18]. In the literature, a series of CrN/Cr multilayer coatings with different period thicknesses were fabricated to reveal that the decrease in dislocation motion

Available online at <http://link.springer.com/journal/40195>.

✉ Zhiliang Pei
zlpei@imr.ac.cn

✉ Chao Sun
csun@imr.ac.cn

¹ Shi-Changxu Innovation Center for Advanced Materials, Institute of Metal Research, Chinese Academy of Sciences, Shenyang 110016, China

² School of Materials Science and Engineering, University of Science and Technology of China, Shenyang 110016, China

and generation within layers resulting from the decrement of period thickness could enhance the hardness of the coating [19]. Cheng et al. reported [20] that the Ti layer thickness could influence the mechanical and tribological properties of TiN/Ti coatings due to the existence of lattice mismatches in the boundaries between Ti and TiN layers, which will inhibit the movement of dislocation. Beyond that, TiN/Ti coatings can improve the hardness while conserving good fracture toughness compared to monolayer coatings [20]. Previous works have focused on the multilayer films of AlB₂-type WB₂ [12, 21], though studies about multilayer coatings containing amorphous WB₂ and metal coatings are rare. The metal Ti interlayer is widely considered because of its impact on the mechanical and tribological properties of the coatings. Accordingly, multilayer coatings composed of amorphous WB₂ and metal Ti sublayers are prepared, and the microstructure and properties of the coatings are investigated.

In this work, WB₂/Ti multilayer coatings were fabricated by direct current (DC) magnetron sputtering. The effect of modulation ratio and bilayer number on the microstructure, mechanical, and tribological properties of the multilayer coatings was systematically studied. This work will provide a new angle of view for further research on WB₂-based coatings with excellent properties.

2 Experimental

2.1 Coating deposition

The WB₂/Ti multilayer coatings with different modulation ratios and periods were deposited using a homemade dual-target DC magnetron sputtering system. A WB₂ target (99.9% purity, 270 mm × 70 mm × 7 mm) and a Ti target (99.9% purity, 270 mm × 70 mm × 7 mm) arranged at a tilt angle of 120° were connected to a DC power supply (MDX-1.5 K, Advanced Energy, USA) and a pulsed DC power supply (Pulse Tech, China), respectively. Mirror-polished YG8 cement carbide (20 mm × 20 mm × 2 mm) substrates were used for XRD characterization and the measurement of mechanical and tribological behaviors. (100) Si wafer (25 mm × 5 mm × 0.5 mm) substrates were used for scanning electron microscope (SEM) morphology observation and indentation toughness measurement. Prior to the deposition, the substrates were ultrasonically cleaned in acetone and ethanol for 15 min sequentially and dried with N₂ gas.

The base pressure of the chamber was under 4×10^{-3} Pa. To remove contaminants, the substrates were ion-etched by Ar⁺ with a bias voltage of −1000 V at 3.0 Pa for 30 min. The deposition pressure was 0.7 Pa in Ar (99.999%) atmosphere. The sputtering power of the WB₂ target and Ti target was 200 W and 270 W, respectively. The substrates were applied

with a bias voltage of −50 V, and the distance between substrates and targets was fixed at 70 mm. During the deposition, the chamber temperature was kept at 200 °C. The WB₂/Ti multilayer coatings with different modulation ratios and bilayer numbers were obtained by alternatively controlling the sputtering time of each target, and the details of deposition time are listed in Table 1. There are two groups of WB₂/Ti multilayer coatings: in group 1, the bilayer number of the coatings was set to be 10, and the modulation ratios, which are the sublayer thickness ratios of WB₂ to Ti, were 1, 5, 15, and 30 and were named S1–S4, respectively; in group 2, the modulation ratio was set to be 5, and the bilayer numbers were 10, 20, 30, 50, and 70, and the coatings with different bilayer number were named S21–S24 besides S2, respectively, as listed in Table 2.

2.2 Characterization

The phase composition of the coatings was characterized by X-ray diffraction (XRD; D/Max-2500 PC, Rigaku, Japan) using CuK α radiation with $\lambda = 0.154$ nm operated at 50 kV and 100 mA in theta-2 theta scanning mode. A field-emission scanning electron microscope (FE-SEM, Quanta, 200F) equipped with an energy-dispersive X-ray spectrometer (EDS) was used to study the cross-sectional microstructure of the coatings and the wear track morphology after the wear test.

A nanoindenter tester (Nano Indenter G200, KLA-Tencor), equipped with a 20-nm-radius Berkovich diamond tip, was employed to obtain the hardness and Young's modulus of the coatings through continuous stiffness mode (CSM) according to Oliver and Pharr's method [22, 23]. At least 10 indentations were performed on different areas of each sample to eliminate the error. The maximum depth chosen to calculate the average hardness and Young's modulus was less than 10% of the coating thickness to avoid the influence of the substrate effect [24].

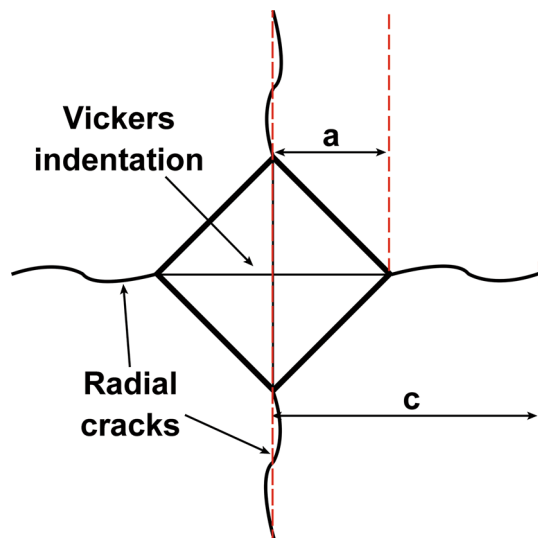
Since it is unavoidable for the influence of substrates during the fracture toughness measurement of coatings [25, 26], a widely applied indentation method [27, 28, 29, 30] was adopted to evaluate the fracture toughness of the multilayer coatings. Precisely, the fracture toughness measured by the

Table 1 Deposition time of WB₂/Ti multilayer coatings

Target	Deposition time in one bilayer (s)			
	S1	S2	S3	S4
WB ₂	148	246	301	306
Ti	1125	375	141	73
WB ₂	123	82	49	35
Ti	188	125	75	54

Table 2 Average values of modulation ratio, bilayer number, H , E , and wear rate (W) of multilayer WB₂/Ti coatings

No.	Modulation ratio	Bilayer number	H (GPa)	E (GPa)	K_{IC} (MPa·m ^{1/2})	W ($\times 10^{-16}$ m ³ /Nm)
S1	1	10	13.9±0.8	193.1±10.2	2.00±0.29	4.73±1.68
S2	5	10	15.8±0.8	203.5±6.2	1.73±0.27	3.38±0.50
S3	15	10	17.9±0.5	230.1±8.1	1.50±0.19	3.70±0.72
S4	30	10	19.2±0.6	254.1±10.0	1.30±0.11	2.96±0.58
S21	5	20	17.0±0.5	220.6±6.1	1.94±0.23	2.62±0.65
S22	5	30	17.9±0.5	235.6±9.8	1.97±0.25	2.52±0.87
S23	5	50	20.4±0.5	256.7±8.9	2.14±0.17	1.76±0.24
S24	5	70	11.8±0.4	156.7±5.1	1.20±0.21	105.76±15.51

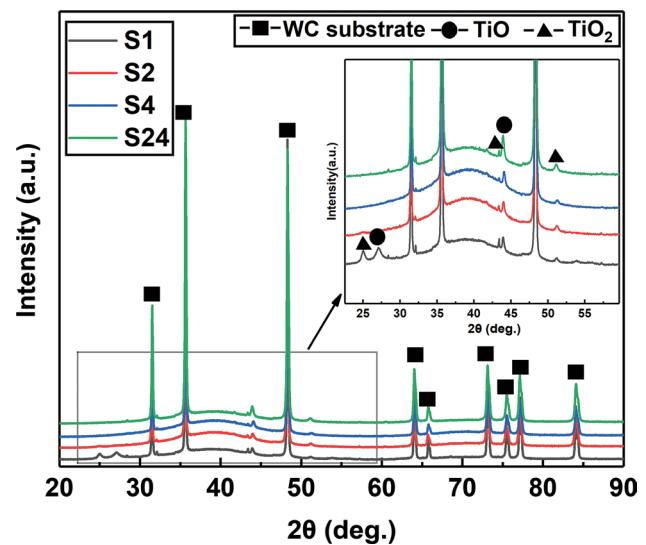
**Fig. 1** Schematic illustration of Vickers indentation

indentation method will be called indentation toughness. A Vickers hardness tester (FM-700, Future-tech) was used to evaluate the indentation toughness of the multilayer coatings under the applied load of 2 N and a hold time of 15 s. The indentation toughness is calculated by the following equation [31]:

$$K_{IC} = \alpha \left(\frac{E}{H} \right)^{\frac{1}{2}} \left(\frac{P}{c^{\frac{3}{2}}} \right), \quad (1)$$

where α is a constant related to the indenter geometry with the value of 0.016 for the Vickers indenter; H and E are the hardness and Young's modulus of the coatings; P is the applied load; c is the radial crack length as shown in Fig. 1.

The tribological properties of the multilayer coatings were carried out by a ball-on-disk tribometer (MS-T3000) against a 4-mm-diameter Al₂O₃ balls counterpart under atmospheric environments at 25 °C, and the relative humidity was 60%. The constant load, rotation speed, rotation radius, and sliding time were set at 0.5 N, 200 r/min, 2.5 mm, and 240 min,

**Fig. 2** XRD patterns of S1, S2, S4, and S24

respectively. A surface profiler (Alpha-Step IQ; KLA-Tencor) was utilized to estimate the wear track profiles after the tribotest. The wear rate (W) was calculated by Archard's classical wear equation [32]:

$$W = \frac{V}{P \times S}, \quad (2)$$

where V is the wear volume of the coatings, P is the applied load, and S is the sliding distance.

3 Results and Discussion

3.1 Microstructure and morphology

Figure 2 shows the XRD patterns of S1, S2, S4, and S24, which represent all the multilayer coating. No diffraction peaks corresponding to WB₂ or Ti can be observed, indicating that all the multilayer coatings show an amorphous structure. This is because the crystallinity of WB₂ coating

is strongly related to the deposition temperature. The multilayer coatings were all fabricated at a relatively low temperature, resulting in the incomplete rearrangement of adsorbed atoms on the grown surface and limiting the extensive growth of crystallites. The crystallization temperature of WB_2 coating is normally beyond $400\text{ }^\circ\text{C}$ [8]. In addition to the diffraction peaks of WC substrates, several weak peaks corresponding to titanium oxides can be observed, denoting that part of the Ti elements have been oxidized by the oxygen in the background vacuum. Besides, a broadband with a typical amorphous character ranging from 25° to 55° can be found in each pattern, indicating that the coatings exhibit amorphous phases with no long-range ordered structure. The full widths at half maximum (FWHMs) of all the patterns are about 14, denoting that there is little change in the short-range order of the amorphous structure for the coatings. Moreover, there is no increased intensity corresponding to the d -spacing position of Ti or WB_2 .

Figure 3 presents the cross-sectional morphologies of the WB_2 /Ti multilayer coatings. The light and relatively dark sublayers represent WB_2 and Ti layers. The coating thickness of S1, S2, S3, and S4, which have the same bilayer number of 10, is about $1.6\text{--}1.7\text{ }\mu\text{m}$, and the modulation ratios of the coatings are basically the same as the design of multilayers, as shown in Fig. 3a–d. As for S21, S22, S23, and S24 in Fig. 3e–i, the modulation ratio is set as 5, and the bilayer numbers are 20, 30, 50, and 70, respectively. All sublayers of the multilayer coatings adhere well, and no obvious defects can be found at the interfaces or the layers.

3.2 Mechanical properties

3.2.1 Effect of modulation ratio

Firstly, WB_2 /Ti multilayer coatings with a fixed bilayer number of 10 and different modulation ratios were

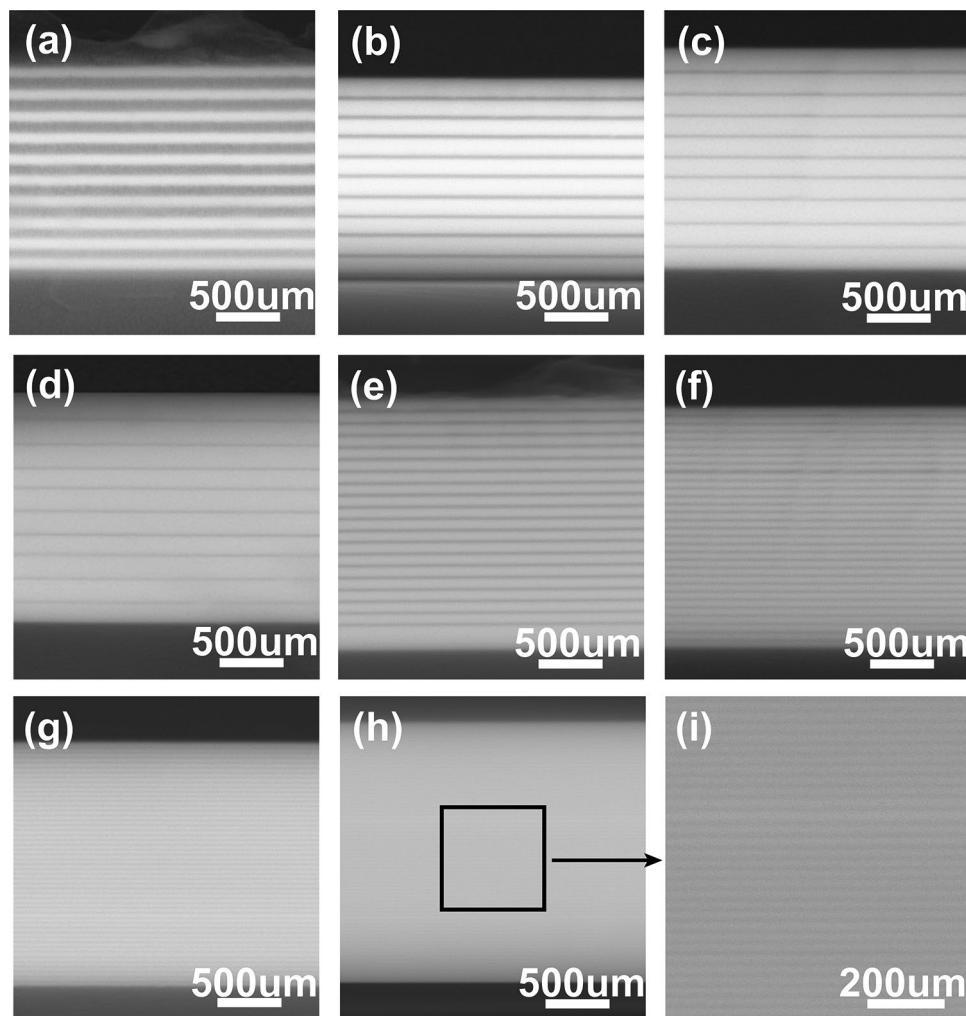


Fig. 3 Cross-sectional morphologies of the WB_2 /Ti multilayer coatings: **a** S1, **b** S2, **c** S3, **d** S4, **e** S21, **f** S22, **g** S23, **h** S24, **i** partial enlarged image of S24

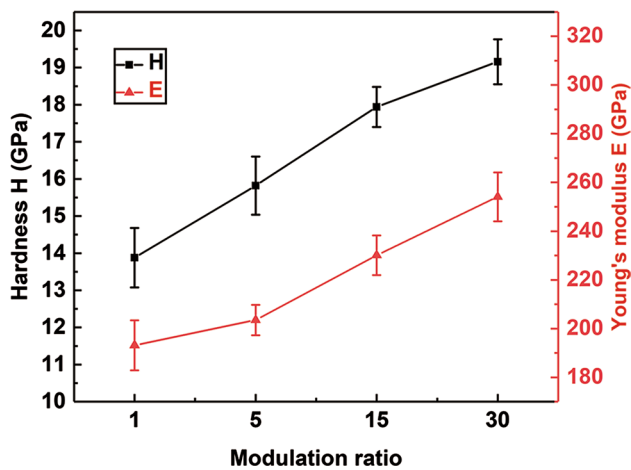


Fig. 4 Hardness and Young's modulus of S1–S4 as a function of modulation ratio

fabricated, which are S1, S2, S3, and S4, and the hardness (H) and Young's modulus (E) of them are shown in Fig. 4 and Table 2 as a function of modulation ratio. It can be easily found that the hardness of WB₂/Ti multilayer coatings is strongly related to the modulation ratio. The highest and lowest hardness of the multilayer coating is achieved at the coating with a modulation ratio of 30 and 1, and the value of 19.2 GPa and 13.9 GPa, respectively, which is the hardness of the multilayer coating, increases with the increment of modulation ratio. This could be understood as the hardness of WB₂/Ti multilayer coatings increases with the volume fraction of the WB₂ sublayer, since the hardness of WB₂ and Ti monolayer fabricated under the same deposition parameters is 20.2 ± 1.2 GPa and 11.6 ± 1.2 GPa, separately. However, it is obvious that even the hardness of S4 is lower than that of WB₂; in another word, the multilayer structures provide no hardness enhancement. Generally speaking, the interfaces between the sublayers could improve the hardness of the multilayer coatings by blocking the dislocation motion [33]. Nonetheless, the thickness of the sublayers of S1–S4 is over 70 μm ; as a result, the dislocation can slide inside the sublayer, resulting in the absence of interfacial effect [34]. Accordingly, the hardness of WB₂/Ti multilayer coatings increases with the increase in the volume ratio of WB₂ sublayer, which provides better resistance to plastic deformation.

The relationship between the indentation toughness and hardness of S1–S4 is shown in Fig. 5. The indentation toughness of S1–S4 shows a nearly linear opposite trend to the hardness with the increase in modulation ratio. As the modulation ratio decreases, the indentation toughness of the multilayer coatings increases from $1.30 \text{ MPa m}^{1/2}$ to $2.00 \text{ MPa m}^{1/2}$ with the increment of ductile Ti metal volume fraction. This is mainly ascribed to the crack bridging

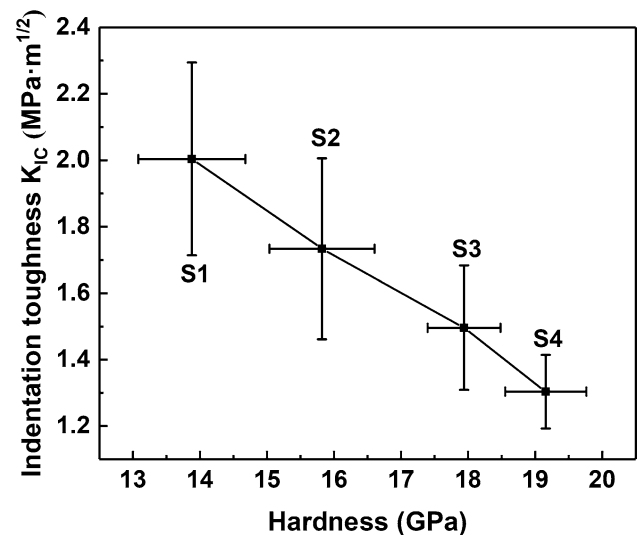


Fig. 5 Relationship between indentation toughness and hardness of S1–S4 with different modulation ratios

behind the cracks of the ductile phase, which absorbs the plastic deformation energy [35].

3.2.2 Effect of bilayer number

From the results above, with the increase in modulation ratio, the hardness of the multilayer coatings increases, while the indentation toughness decreases. Consequently, to balance the hardness and toughness, the effect of bilayer number on the properties of WB₂/Ti multilayer coatings was studied with a modulation ratio of 5.

Figure 6 presents the hardness and Young's modulus of S2, S21, S22, S23, and S24 with different bilayer numbers as a function of bilayer number. With the increase in bilayer number from 10 to 50, the hardness of WB₂/Ti multilayer coatings increases from 15.8 GPa to 20.4 GPa, and the hardness of S23 with the bilayer number of 50 is at the same level as that of pure amorphous WB₂ monolayers coating (20.2 GPa), whereas, with the further increment of bilayer number to 70, the hardness of the coating decreases rapidly to 11.8 GPa. Furthermore, Young's modulus exhibits a similar changing tendency. The increasing hardness of the coatings is mainly attributed to the periodic multilayer structure. The dislocation movement can be impeded by the interfaces between the sublayers and the formation of dislocation pileup at the interfaces could improve the yield strength, inducing the enhancement of hardness of the multilayer coatings [36, 37]. It is well known that the hardness enhancement resulting from the multilayered structure effect is owing to the difference in shear modulus [34]. The shear modulus of WB₂ and Ti monolayer coatings can be calculated by the following equation:

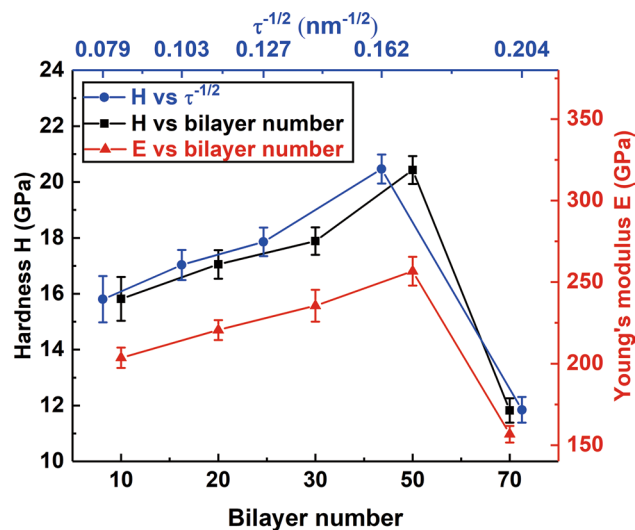


Fig. 6 Hardness and Young's modulus of S2, S21, S22, S23, and S24 as a function of bilayer number and relationship between hardness and $\tau^{-1/2}$

$$G = \frac{E}{2(1 + \nu)}, \quad (3)$$

where G is the shear modulus, E is Young's modulus, and ν is the Poisson ratio. The Young's modulus of amorphous WB_2 monolayer coating deposited at the same condition is measured to be 236.54 ± 8.76 GPa, and the Poisson ratio of WB_2 is 0.27 [38]. The Young's modulus and Poisson ratio of Ti are 134 GPa and 0.25, respectively [39]. The shear modulus of WB_2 and Ti is calculated to be 93.13 GPa and 53.6 GPa, respectively, so the disparity between them could cause the multilayer effect. Besides, according to Yashar and Sproul's work, in multilayered structure coatings, dislocations tend to remain in the sublayers with lower shear modulus, and extra stress is demanded for the movement of dislocations to sublayers with higher shear modulus [40]. They proposed an equation using a Hall–Petch approach model:

$$H_m = H_0 + k\tau^{-1/2}, \quad (4)$$

where H_m is the hardness of the multilayer coatings; H_0 is the hardness from the sublayers; k is a parameter related to the interfaces; and τ is the modulation period of the multilayer coatings. Relationship between the hardness and $\tau^{-1/2}$ of S2, S21, S22, S23, and S24 is shown in Fig. 6. For S2–S23, the hardness of the coatings nearly increases linearly with $\tau^{-1/2}$. Hence, it can be concluded that the hardness enhancement of the coatings is indeed induced by the multilayer effect. However, the hardness of S24 did not match this model. This can be ascribed to that the ion bombardment could give rise to interface diffusion during deposition, especially for the thinner Ti sublayers, which is difficult to form strong

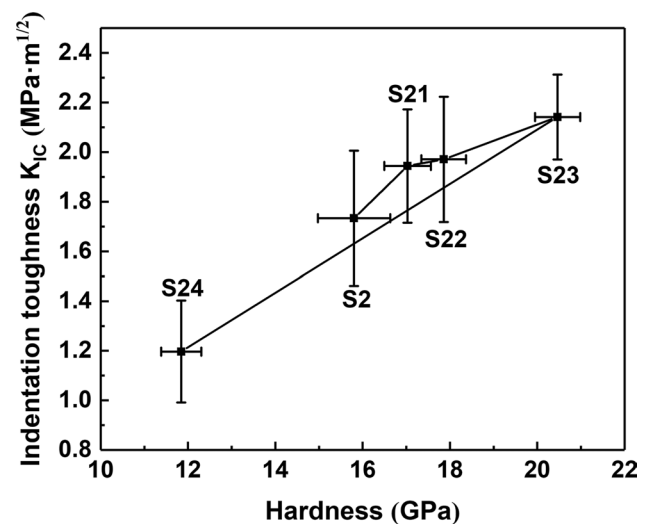


Fig. 7 Relationship between indentation toughness and hardness of S2, S21, S22, S23, and S24 with different bilayer numbers

interfaces, leading to the weakening of the interface effect and the decrease in hardness [41]. Similar work of Ti/TiN multilayer coatings has been reported by Li et al. [42].

Relationship between the indentation toughness and hardness of WB_2/Ti multilayer coatings with different bilayer numbers is shown in Fig. 7. Normally, the hardness and toughness of materials are inversely proportional, whereas for S2–S23, both indentation toughness and hardness increase with the increment of bilayer number. The indentation toughness of the multilayer coatings increases from $1.73 \text{ MPa m}^{1/2}$ to $2.14 \text{ MPa m}^{1/2}$ with the increment of bilayer number from 10 to 50. It can be speculated that the contribution of the interfaces deeply influences the indentation toughness of the coatings. The elastic modulus differences between WB_2 (236.54 GPa) and Ti (134 GPa) could generate interfacial effect, which can block the crack propagation across the coatings by lateral crack deflection [43, 44], leading to the improvement of indentation toughness of the multilayer coatings. Nevertheless, as the bilayer number reaches 70, the influence of interfaces diminishes due to the interface diffusion effect described above, giving rise to the decrease in both the indentation toughness and hardness of the coating.

3.3 Tribological properties

Figure 8 shows the friction coefficient curves of S1, S2, S3, and S4 with different modulation ratios versus the sliding time. A standard running-in period can be observed at the beginning of the test. The friction coefficient changes abruptly and fluctuates due to the presence of some extraneous contaminants and oxides [45]. Then, the friction coefficient decreases to a lower value. This is mainly because

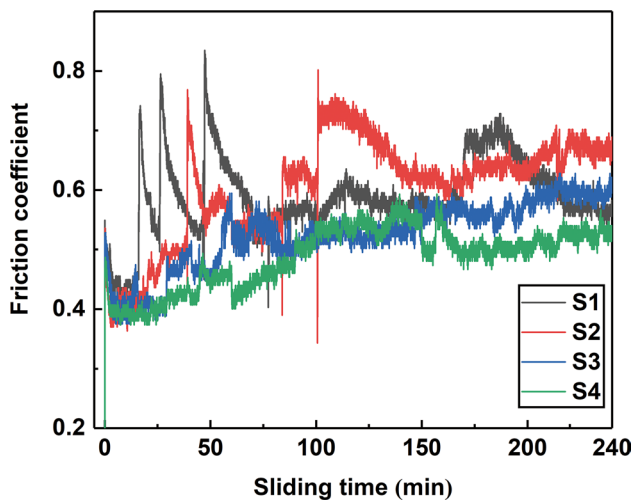


Fig. 8 Friction coefficient curves of S1, S2, S3, and S4 as a function of sliding time

WB₂ coatings can produce lubricant boric and tungsten oxides, leading to the decrement of friction coefficient [8]. Subsequently, some hard WB₂ wear debris particles could not leave the wear track immediately and will slide with the lubrication media, resulting in the gradual increase in friction coefficient [46]. After that, the friction coefficient shows different changing tendencies based on the different structures and mechanical properties of the multilayer coatings. The friction coefficient of S1 presents fast and frequent fluctuations. The rapid increase in friction coefficient represents that the worn surface switches from the hard WB₂ to soft Ti sublayers, and with the quickly worn-out of soft Ti sublayers, the friction coefficient decreases afterward. As the wear test proceeds, more lubrication media are produced, and accordingly, the friction coefficient curve tends to reach a relatively stable state. The friction coefficient of S2 fluctuates later than that of S1 and has a lower frequency. This is because that S2 has higher hardness and thicker thickness of WB₂ sublayers, which makes the WB₂ sublayer be worn out slower than S1. As for S3 and S4 with higher modulation ratios, the friction coefficient curves remain in a relatively stable state. This is due to the thinner thickness of Ti sublayers, and thereby the switching process between WB₂ and Ti sublayers can be accomplished in a short time.

The wear rate and average friction coefficient of S1, S2, S3, and S4 are presented in Fig. 9. S4 exhibits the lowest wear rate of $2.96 \times 10^{-16} \text{ m}^3/\text{Nm}$ among S1–S4. This can be due to the wear property is usually related to the hardness in terms of the Archard theory [32]. However, S2 and S3 have similar wear rates while having different hardness, which may be ascribed to the better fracture toughness of S2. The cross-sectional profile of the wear tracks is also presented in Fig. 9. The wear track of S1 is broader and shallower than

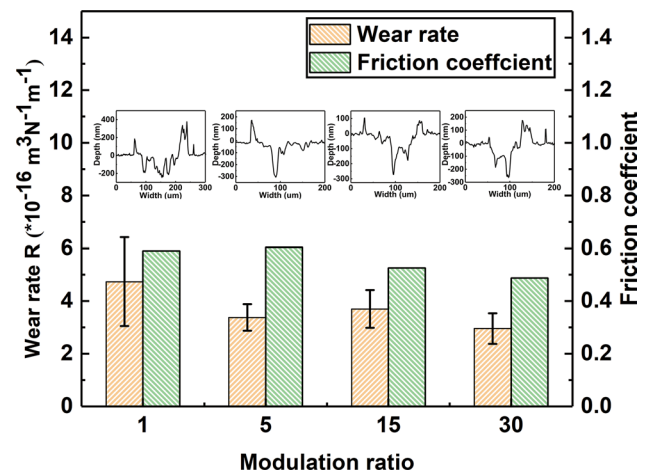


Fig. 9 Wear rate, average friction coefficient, and cross-sectional profile of the wear tracks for S1, S2, S3, and S4

that of the others. Furrows can be observed in all the wear tracks, indicating that the main wear mechanism of WB₂/Ti multilayer coatings is abrasive wear.

Figure 10 shows the wear track morphologies of S1, S2, S3, and S4. The wear track of S1 has the broadest width, and the wear track widths of the coatings present a decreasing trend with the increase in modulation ratio. This is mainly due to the increment of hardness, which decreases the plastic deformation of the contact area. Furrows parallel to the wear tracks can be observed in all the multilayer coatings, which is caused by the abrasive ploughing of hard WB₂ wear debris, denoting that the main wear mechanism of the multilayer coatings during the dry sliding is abrasive wear [47]. The wear track widths of S3 and S4 are narrower than S1, whereas cracks can be observed in S3, and irregular delamination occurs in the wear track of S4. With the increase in modulation ratio, the decrease in ductile Ti metal volume fraction gives rise to the decrement of fracture toughness for the multilayer coatings. During the sliding process, the slide between the counterparts could cause the formation of fatigue tensile cracks, and the accumulation of cracks may lead to the peeling off of some fragments. As discussed above, the indentation toughness of S3 is lower than that of S1 and S2, which makes it difficult to restrain the formation and propagation of the fatigue tensile cracks. As for S4 with the lowest indentation toughness of $1.30 \text{ MPa}\cdot\text{m}^{1/2}$, the accumulation of cracks causes fragment peeling and produces delamination. Even though the wear track of S1 is relatively smooth and without cracks or peeling off, the severe abrasive wear induced by low hardness makes it to maintain the highest wear rate. Furthermore, EDS is also undertaken to analyze the chemical composition inside the wear tracks of S1–S4. The result shows that O, Ti, and W exist in all the wear tracks, indicating that the penetration depth during the

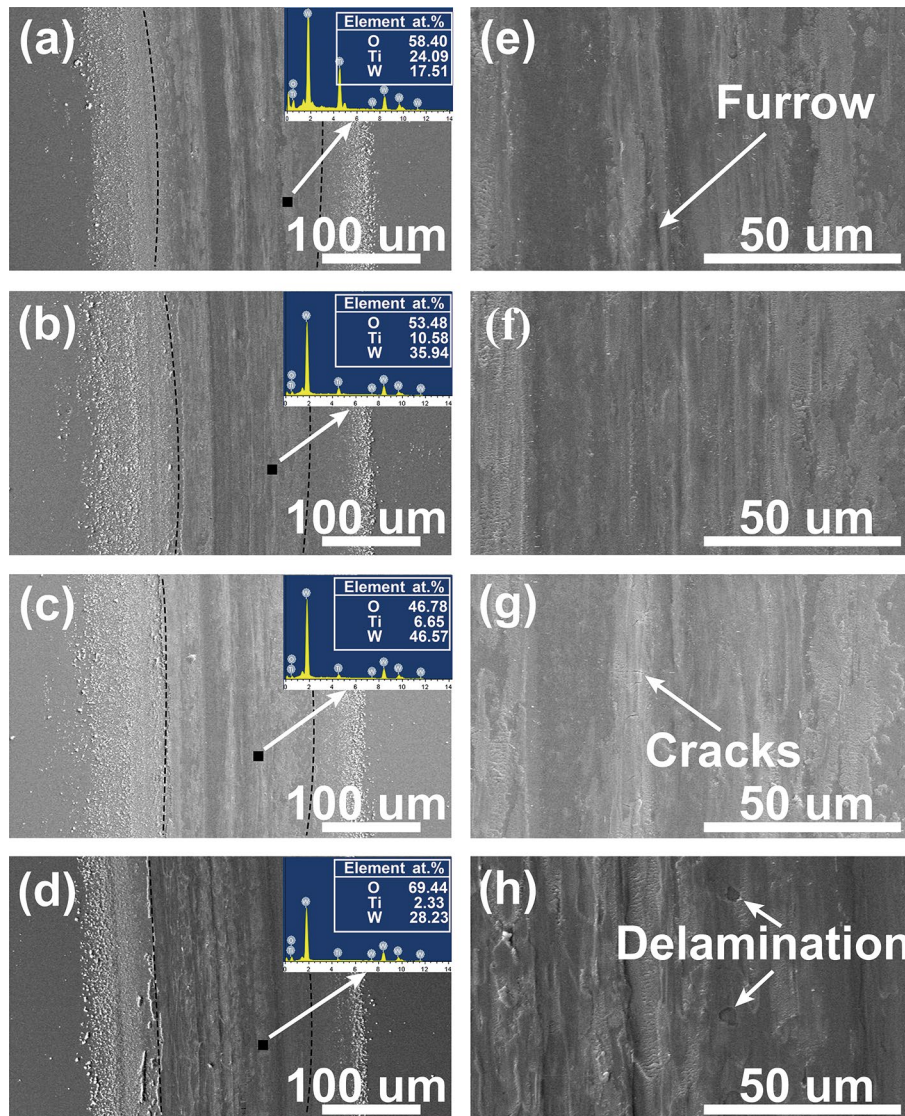


Fig. 10 Wear track morphologies of **a** S1; **b** S2; **c** S3; **d** S4 and enlarged images of **e** S1; **f** S2; **g** S3; **h** S4

wear test exceeds more than one modulation period thickness for all the coatings. Thereinto, the worn-out of one sublayer could induce the fluctuation of the friction coefficient. The Ti content in the wear tracks decreases with the increase in modulation ratio due to the decrease in Ti sublayer volume ratio. Besides, the huge amount of oxygen denotes the formation of oxides during the dry sliding process, which is in accordance with the result above. B is out of detection due to its light mass, and no existence of Al indicates that there is no material transfer from Al_2O_3 balls to the multilayer coatings.

Figure 11 shows the friction coefficient curves of S2, S21, S22, S23, and S24 with different bilayer numbers. For the multilayer coatings with bilayer number of no more than 50, the friction coefficients fluctuate at a similar level. In addition, the friction coefficient curve fluctuation of S21–S23 is

less than that of S2, which could be attributed to the increment of bilayer number. With the increase in bilayer number, the decrease in modulation period and Ti sublayer thickness could reduce the friction coefficient fluctuation during the switch between different sublayers [21].

Figure 12 presents the wear rate, average friction coefficient, and cross-sectional profile of the wear tracks. As the bilayer number of the multilayer coatings increases from 10 to 50, the wear rate of the coatings decreases, owing to the increment of both hardness and indentation toughness, and S23 with the bilayer number of 50 exhibits the lowest wear rate of $1.76 \times 10^{-16} \text{ m}^3/\text{Nm}$ due to its highest hardness and indentation toughness. As for S24 with bilayer number of 70, both the friction coefficient and wear rate display a higher value than those of the other samples. This is because the coating has been depleted during the wear test due to its poor

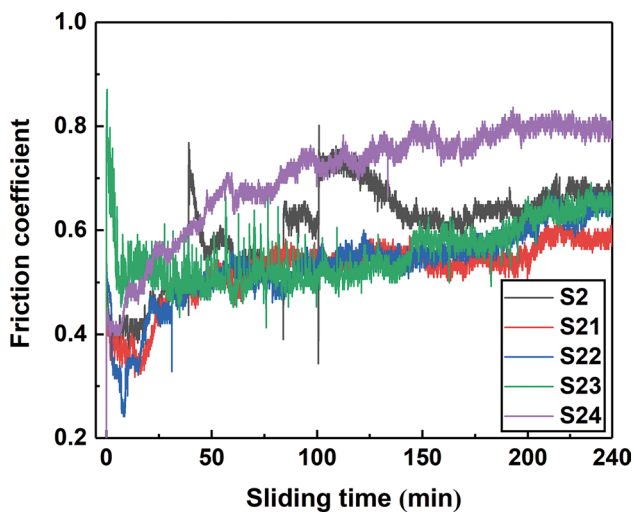


Fig. 11 Friction coefficient curves of S2, S21, S22, S23, and S24 as a function of sliding time

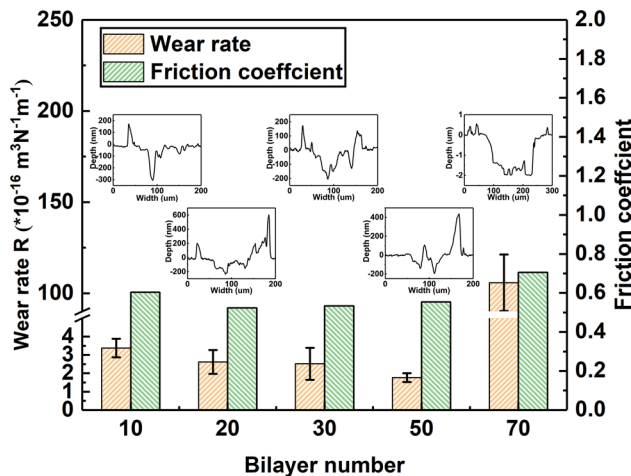


Fig. 12 Wear rate, average friction coefficient, and cross-sectional profile of the wear tracks for S2, S21, S22, S23, and S24

hardness and indentation toughness, and the worn surface switches from the multilayer coating to the substrate. It can be found in the cross-sectional profile of the wear tracks that the wear tracks become narrower and shallower with the increase in bilayer number from 10 to 50, due to the increase in coating hardness and indentation toughness. The wear track of S24 is much deeper and broader than that of the others, which confirms that the coating has been worn out during the test.

Wear track images of S21, S22, S23, and S24 are presented in Fig. 13 for further investigation of their tribological properties. Furrows parallel to the wear tracks can also be observed in all the multilayer coatings, indicating that the wear mechanism of the multilayer coatings has not

changed with the increase in bilayer number. No cracks or delamination can be observed in the wear tracks of S21, S22, and S23, declaring good fracture toughness, as discussed above. Besides, while the bilayer number is no more than 50, the wear track widths of the coatings decrease with the increase in bilayer number due to the increment of coatings hardness, which is in accordance with the result above. For S24 as shown in Fig. 12d, the porous YG8 cement carbide substrate can be observed, indicating the total delamination of the coating. Besides, many severe cracks exist in the remained coating. This also certifies the poor hardness and fracture toughness of the coating. EDS is also conducted to investigate the chemical composition in the wear tracks for S2–S23. O, Ti, and W exist in all the wear tracks, denoting the formation of oxides during the test, and the Ti content is at the same level for all the coatings owing to the similar Ti sublayer volume ratio.

4 Discussion

Both hardness and indentation toughness could influence the wear resistance of the coatings. Comparing the wear rate of S1–S4 with different modulation ratios as shown in Fig. 9, coatings with higher hardness exhibit better ability to resist plastic deformation during contact with the counterpart and reduce the friction area and wear rate [48]. Whereas the lower toughness of the coating tends to generate more cracks, inducing more peeling off of hard particles and some irregular delamination could occur. Moreover, some hard particles may slide or roll with the sliding of the counterpart, aggravating the abrasive wear and increasing the wear rate. Therefore, the wear rates of S1–S4 are at the same level owing to the inverse changing tendency of hardness and toughness with the increase in modulation ratio. As for S2–S23 with different bilayer numbers, relatively high toughness and no cracks or delamination exists in the wear track, and the increase of coating hardness leads to the decrease in wear rate.

In summary, a wear mechanism schematic diagram of WB₂/Ti multilayer coatings is shown in Fig. 14. As the wear test begins, the counterparts contact directly with WB₂ sublayer and the Al₂O₃ ball, and local deformation occurs in the wear track, as shown in Fig. 14a. Then, lubricant boric and tungsten oxides are formed at the contact area due to the local high temperature caused by dry sliding, and some loose hard WB₂ particles may slide along with the lubrication media and act as abrasive debris. At the same time, fatigue tensile cracks appear due to the brittleness of the WB₂ sublayer and would propagate to the sublayers below, as shown in Fig. 14b. As more cracks reach the Ti sublayer, the WB₂ sublayer would delaminate quickly and generate more hard abrasive debris, which

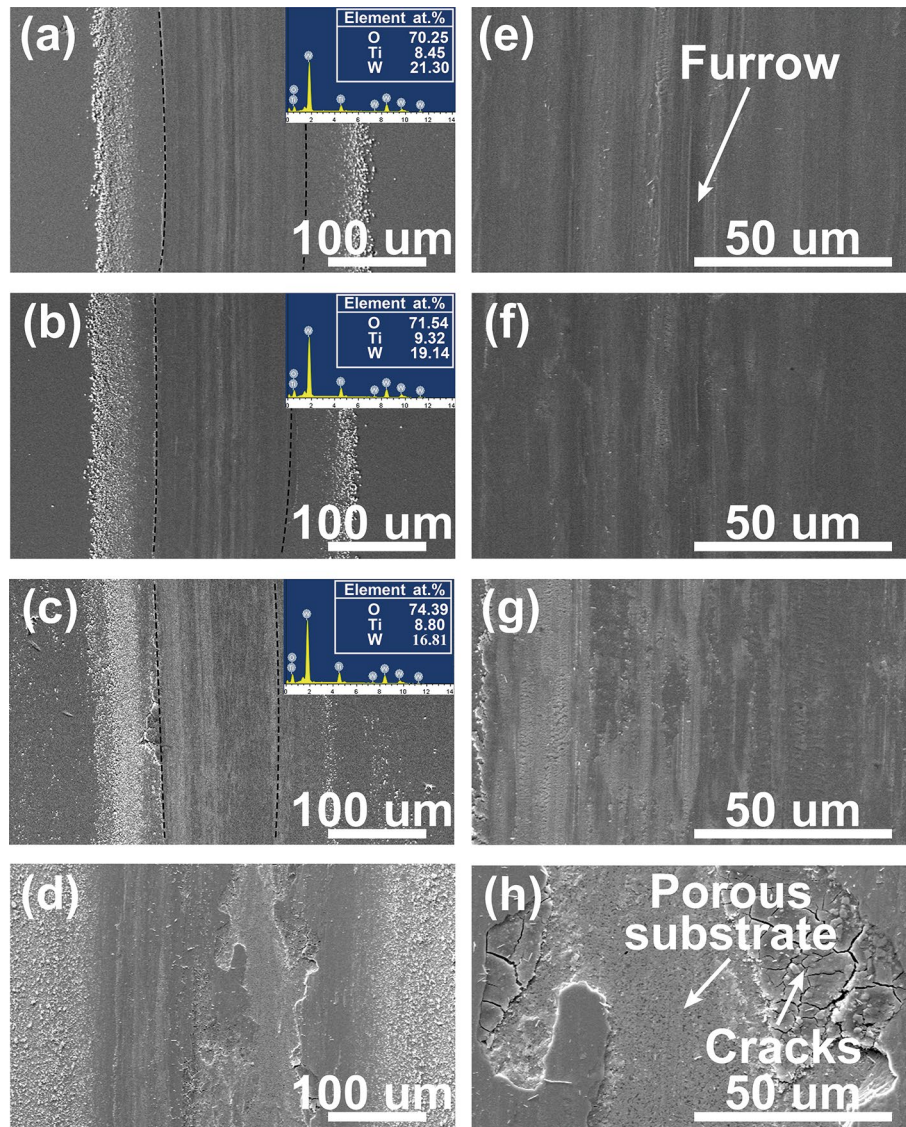


Fig. 13 Wear track morphologies of **a** S21; **b** S22; **c** S23; **d** S24, and enlarged images of **e** S21; **f** S22; **g** S23; **h** S24

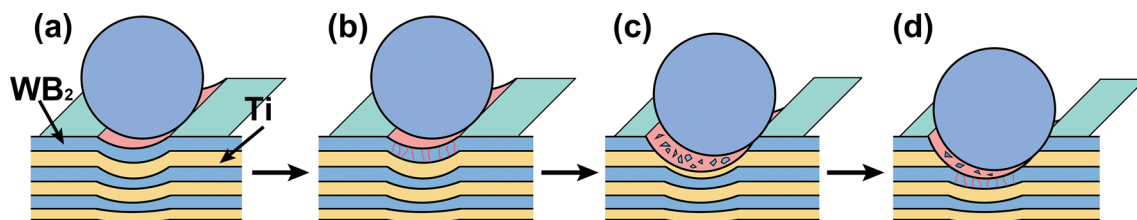


Fig. 14 Schematic diagram of wear mechanism of WB_2/Ti multilayer coatings

will accelerate the removal of the soft Ti sublayer, as shown in Fig. 14c. After the Ti sublayer being totally removed, the counterparts become Al_2O_3 ball and a brand-new WB_2 sublayer, and the process mentioned above will continue repeatedly [49]. It can be summarized that

abrasive wear domains the wear mechanism of amorphous WB_2/Ti multilayer coatings, besides, slight oxidation wear exists simultaneously. With the adjustment of modulation ratio and bilayer number, the improvement of hardness and indentation toughness of the multilayer coatings could

effectively resist plastic deformation and hinder the propagation of cracks at the same time.

5 Conclusion

Amorphous WB₂/Ti multilayer coatings with different modulation ratios (1, 5, 15, and 30) and bilayer numbers (10, 20, 30, 50, and 70) have been deposited on YG8-cemented carbides and (100) Si wafers by magnetron sputtering. The effects of modulation ratio and bilayer number on the microstructure, mechanical, and tribological properties of WB₂/Ti multilayer coatings are investigated in detail.

For the investigation of the influence of modulation ratio, the bilayer number of the multilayer coatings is set as 10. The hardness of the coatings increases with the increment of modulation ratio ranging from 13.9 GPa to 19.2 GPa, while the indentation toughness shows a different changing tendency. The mechanical properties of the multilayer coatings with different modulation ratios are basically decided by the volume ratio of WB₂ and Ti sublayers. Coating with the modulation ratio of 30 exhibits lower wear rate of $2.96 \times 10^{-16} \text{ m}^3/\text{Nm}$ than that of the other coatings mainly due to its high hardness.

For the investigation of the influence of bilayer number, the modulation ratio of the multilayer coatings is set as 5 to balance the hardness and indentation toughness. Both hardness and indentation toughness increase with the bilayer number increase from 10 to 50 and reach the maximum value of 20.4 GPa and $2.14 \text{ MPa}\cdot\text{m}^{1/2}$ with the bilayer number of 50, whereas as the bilayer number reaches 70, the mechanical properties of the multilayer coating decrease rapidly due to the weakening of the interface effect. Amorphous WB₂/Ti multilayer coating with the modulation ratio of 5 and bilayer number of 50 presents the best wear resistance owing to its excellent mechanical properties.

Acknowledgements This work was supported by the Shi-Changxu Innovation Center for Advanced Materials.

Declarations

Conflict of interest The authors state that there are no conflicts of interest to disclose.

References

- [1] S. Vepřek, *J. Vac. Sci. Technol. A* **17**, 2401 (1999)
- [2] R.B. Kaner, J.J. Gilman, S.H. Tolbert, *Science* **308**, 1268 (2005)
- [3] C. Jiang, Z. Pei, Y. Liu, J. Xiao, J. Gong, C. Sun, *Phys. Status Solidi A-Appl. Mat.* **210**, 1221 (2013)
- [4] S.C. Zhang, Z.Y. Wang, P. Guo, P.L. Ke, M. Oden, A.Y. Wang, *Surf. Coat. Technol.* **322**, 134 (2017)
- [5] R. Hahn, A. Tymoszuk, T. Wojcik, A. Kirnbauer, T. Kozák, J. Capek, M. Sauer, A. Foelske, O. Hunold, P. Polcik, P.H. Mayrhofer, H. Riedl, *Surf. Coat. Technol.* **420**, 127327 (2021)
- [6] X.F. Hao, Y.H. Xu, Z.J. Wu, D.F. Zhou, X.J. Liu, X.Q. Cao, J. Meng, *Phys. Rev. B* **74**, 224112 (2006)
- [7] E. Zhao, J. Meng, Y. Ma, Z. Wu, *PCCP* **12**, 13158 (2010)
- [8] Y.M. Liu, C.L. Jiang, Z.L. Pei, H. Lei, J. Gong, C. Sun, *Surf. Coat. Technol.* **245**, 108 (2014)
- [9] Y.M. Liu, D.Y. Deng, H. Lei, Z.L. Pei, C.L. Jiang, C. Sun, J. Gong, *J. Mater. Sci. Technol.* **31**, 1217 (2015)
- [10] Y.M. Liu, Z.L. Pei, J. Gong, C. Sun, *Surf. Coat. Technol.* **291**, 276 (2016)
- [11] Y.M. Liu, T. Li, F. Liu, Z.L. Pei, *Acta Metall. Sin.-Engl. Lett.* **32**, 136 (2019)
- [12] W.B. Shi, Y.M. Liu, W.H. Li, J.H. Liu, H. Lei, J. Gong, C. Sun, *Ceram. Int.* **47**, 19678 (2021)
- [13] J. Musil, *Surf. Coat. Technol.* **125**, 322 (2000)
- [14] Y.F. Wang, Z.X. Li, H.N. Wang, J.H. Du, C.W. Zhang, *Rare Met. Mater. Eng.* **46**, 1219 (2017)
- [15] J.B. Santaella-González, J. Hernández-Torres, J. Morales-Hernández, N. Flores-Ramírez, C. Ferreira-Palma, R.C. Rodríguez-Jiménez, L. García-González, *Mater. Lett.* **316**, 132037 (2022)
- [16] P. Wiciniński, J. Smolik, H. Garbacz, K.J. Kurzydowski, *Surf. Coat. Technol.* **240**, 23 (2014)
- [17] X. Cai, Y. Gao, F. Cai, L. Zhang, S. Zhang, *Appl. Surf. Sci.* **483**, 661 (2019)
- [18] J. Shuai, X. Zuo, Z. Wang, L. Sun, R. Chen, L. Wang, A. Wang, P. Ke, *J. Mater. Sci. Technol.* **80**, 179 (2021)
- [19] E. Martínez, J. Romero, A. Lousa, J. Esteve, *J. Phys. D: Appl. Phys.* **35**, 1880 (2002)
- [20] Y.H. Cheng, T. Browne, B. Heckerman, C. Bowman, V. Gorokhovskiy, E.I. Meletis, *Surf. Coat. Technol.* **205**, 146 (2010)
- [21] W.B. Shi, Y.M. Liu, W.H. Li, T. Li, H. Lei, J. Gong, C. Sun, *Acta Metall. Sin.-Engl. Lett.* **35**, 693 (2022)
- [22] W.C. Oliver, G.M. Pharr, *J. Mater. Res.* **7**, 1564 (1992)
- [23] G.M. Pharr, W.C. Oliver, F.R. Brotzen, *J. Mater. Res.* **7**, 613 (1992)
- [24] R. Saha, W.D. Nix, *Acta Mater.* **50**, 23 (2002)
- [25] S. Zhang, D. Sun, Y. Fu, H. Du, *Surf. Coat. Technol.* **198**, 74 (2005)
- [26] S. Zhang, X.M. Zhang, *Thin Solid Films* **520**, 2375 (2012)
- [27] C.L. Jiang, H.L. Zhu, K.S. Shin, Y.B. Tang, *Thin Solid Films* **632**, 97 (2017)
- [28] X.D. Sui, G.J. Li, C.J. Jiang, K. Wang, Y.J. Zhang, J.Y. Hao, Q. Wang, *Ceram. Int.* **44**, 5629 (2018)
- [29] Y.X. Ou, X.P. Ouyang, B. Liao, X. Zhang, S. Zhang, *Appl. Surf. Sci.* **502**, 144168 (2020)
- [30] Y. Yamada, M. Murashima, N. Umehara, T. Tokoroyama, W.Y. Lee, H. Takamatsu, Y. Tanaka, Y. Utsumi, *Tribol. Int.* **169**, 107486 (2022)
- [31] D.B. Marshall, B.R. Lawn, A.G. Evans, *J. Am. Ceram. Soc.* **65**, 561 (1982)
- [32] J.F. Archard, *J. Appl. Phys.* **24**, 981 (1953)
- [33] B. Xiao, T.F. Zhang, Z. Guo, Z. Li, B. Fan, G. Chen, Z. Xiong, Q. Wang, *Surf. Coat. Technol.* **433**, 128094 (2022)
- [34] J.S. Koehler, *Phys. Rev. B* **2**, 547 (1970)
- [35] S. Zhang, D. Sun, Y. Fu, H. Du, *Surf. Coat. Technol.* **198**, 2 (2005)
- [36] X. Chu, S.A. Barnett, *J. Appl. Phys.* **77**, 4403 (1995)
- [37] Y. Zhao, G. Lin, J. Xiao, H. Du, C. Dong, L. Gao, *Appl. Surf. Sci.* **257**, 2683 (2011)
- [38] C.L. Jiang, Z.L. Pei, Y.M. Liu, H. Lei, J. Gong, C. Sun, *Appl. Surf. Sci.* **288**, 324 (2014)
- [39] J.D. Bressan, A. Tramontin, C. Rosa, *Wear* **258**, 115 (2005)
- [40] P.C. Yashar, W.D. Sproul, *Vacuum* **55**, 179 (1999)
- [41] D.M. Mattox, *J. Vac. Sci. Technol. A* **7**, 1105 (1989)
- [42] T.S. Li, H. Li, F. Pan, *Surf. Coat. Technol.* **137**, 225 (2001)

- [43] M.Y. He, A.G. Evans, J.W. Hutchinson, *Int. J. Solids Struct.* **31**, 3443 (1994)
- [44] Y.X. Wang, S. Zhang, *Surf. Coat. Technol.* **258**, 1 (2014)
- [45] T.G. Wang, Y. Dong, B.A. Gebrekidan, Y.M. Liu, Q.X. Fan, K.H. Kim, *Acta Metall. Sin.-Engl. Lett.* **30**, 688 (2017)
- [46] X. Chen, J. Zhang, S. Ma, H. Hu, Z. Zhou, *Acta Metall. Sin.-Engl. Lett.* **27**, 31 (2014)
- [47] J. Zhang, Z. Li, Y. Wang, S. Zhou, Y. Wang, Z. Zeng, J. Li, *Vacuum* **173**, 109158 (2020)
- [48] S.S. Zhao, Y.H. Zhao, L.S. Cheng, V.V. Denisov, N.N. Koval, B.H. Yu, H.J. Mei, *Acta Metall. Sin.-Engl. Lett.* **30**, 176 (2017)
- [49] E. Martínez, J. Romero, A. Lousa, J. Esteve, *Surf. Coat. Technol.* **163–164**, 571 (2003)

Springer Nature or its licensor (e.g. a society or other partner) holds exclusive rights to this article under a publishing agreement with the author(s) or other rightsholder(s); author self-archiving of the accepted manuscript version of this article is solely governed by the terms of such publishing agreement and applicable law.